# Study of the Fermilab Main Injector Lattice

C. S. Mishra and F. A. Harfoush
*Fermi National Accelerator Laboratory**
*Batavia, Illinois 60510*

August 25, 1993

*Abstract*

The Fermilab Main Injector is a new 150 GeV protron synchrotron, designed to remove the limitations of the Main Ring in the delivery of high intensity proton and antiproton beams to the Tevatron. Extensive studies have been made to understand the performance of the Main Injector. In this paper, we present a study of the Main Injector lattice, which includes magnetic and misalignment errors. These calculations show the Main Injector's dynamical aperture being larger than its design value of $40\pi$ mm-mradian at injection. We also discuss a corrrection scheme that reduces the effect of these errors on the performance of the Fermilab Main Injector.

## I. INTRODUCTION

The Fermilab Main Injector (FMI) will be constructed using newly designed conventional dipole magnets and mostly recycled quadrupoles from the Main Ring. The FMI lattice has two different types of cells, the normal FODO cells in the arcs and straight sections and the dispersion-suppressor FODO cells adjacent to the straight sections to reduce the dispersion to zero in the straight sections.

Simulations results of the FMI at its two most critical states, injection at 8.9 GeV and slow extraction at 120 GeV are presented in this paper. The

*Operated by the Universities Research Association under contract with the U.S. Department of Energy

FMI lattice includes the magnetic field errors, both systematic and random, and misalignment errors. Studies of closed orbit errors, betatron function errors, tune versus amplitude and dynamical aperture are also presented. Results show that the dynamical aperture meets the design specifications. A correction scheme which utilizes the octupole and trim quadrupoles will also be discussed. The thin element tracking program TEAPOT [1] has been used for these simulations.

## II. TRACKING CONDITIONS

The Main Injector lattice has two different sizes dipole magnets, their magnetic lengths are 6.096 and 4.064 meters at 120 GeV. The magnetic length of these dipoles varies with energies due to the saturation of ends, and at 8.9 GeV their length is 2.46 mm larger than the nominal length at 120 GeV [2]. This change in length introduces a non zero dipole multipole at each end of the magnet. This additional bending of the particle is corrected by reducing the dipole excitation.

The ends of the magnet have different magnetic multipoles than the body of the magnet. For the tracking calculations the two ends are detached from the body and treated as separate magnets . The dipole body and end multipoles, both normal and skew, are calculated by using the method described in [3]. At present we have only two prototype Main Injector dipoles, so the random errors of the body multipoles are calculated by using the measurements of the similar, existing Main Ring B2 dipoles.

The values of the systematic and random errors of the quadrupoles are calculated using the Main Ring(MR) quadrupole measurements. There are a very limited number of recent measurements available for MR Quads. The Main Ring quadrupoles have a large octupole component and random error. The variation of the octupole strength and random errors with current are small implying a more geometrical effect. All skew quadrupole field errors are turned off for the convenience of the simulation. Using a decoupling scheme any linear coupling effects due to the presence of skew quadrupole can be corrected. Table 1 and 2 summarize all of the multipoles used in the input file to TEAPOT. Details of the input to these tables can be found in reference [3]. Multipole field errors are quoted in units of $10^{-4}$ relative to the main field component and at a displacement of one inch.

The misalignment of all the magnetic elements and beam position monitors are included in this calculation. The RMS of the alignment error with respect to the closed orbit is assumed to be 0.25 mm in both horizontal and

vertical directions. In addition dipole magnets have an RMS roll angle of 0.5 mrad.

Base tunes of $(Q_x, Q_y)$ = (26.425, 25.415) are used in all the simulations. This tune is different from (26.407, 25.409) which was used in earlier calculations. This change in tune was necessary to increase the dynamic aperture with all magnetic and misalignment errors turned on, in the presence of synchrotron oscillations due to RF, and with chromaticity set to the desired value. In the lattice there are 18 RF cavities, each operating at a voltage $V_{rf}$ = 0.0218 MV and 0.0555 MV at 8.9 and 120 GeV respectively. The RF frequency is set to 53 MHz corresponding to a harmonic number 588.

## III. TRACKING RESULTS

### *A. Closed orbit and Betratron Function Errors*

In the Main Injector lattice there are 208 quadrupoles, 128 are recycled Main Ring quadrupoles, while the rest are newly fabricated. Located inside these quadrupoles are the beam position monitors. The vertical and horizontal beam position are measured at the focusing and defocusing quadrupoles respectively. The vertical and horizontal displacement of the particles are corrected by applying corresponding kicks just after these position monitors.

A typical uncorrected closed orbit in both the horizontal and vertical plane is shown in Figure 1. The RMS closed orbit deviation before correction is 5.9 mm horizontally and 4.4 mm vertically for the selected seed. After three iterations of the orbit corrections scheme the RMS closed orbit deviation is reduced to $2.3 \times 10^{-4}$ mm (H) and $7.2 \times 10^{-7}$ mm (V). The correction scheme is based on a least square error minimization. We have studied the contribution of each magnetic error and the displacement error to the RMS closed orbit deviation for one seed. Most of the horizontal closed orbit deviation is due to dipole random strength variations, misalignment errors and the change in the effective length of the dipole magnet. The vertical closed orbit error is mainly due to misalignment errors. Figs 2,3 show the distribution of uncorrected horizontal and vertical RMS closed orbit errors for 20 different seeds at 8.9 and 120 GeV. The RMS deviation of the distribution is 5.0 mm and 3.9 mm in the horizontal and vertical planes respectively.

The maximum corrector strength required to correct these orbit deviations is about 100 $\mu radians$ in both planes at the two considered energies,

as shown in Figure 4. In the Main Injector we plan to use newly built dipole correctors. At 8.9 GeV the Main Injector dipole correctors can provide 2000 $\mu$ radian and 1300 $\mu$ radian of horizontal and vertical corrections respectively.

Due to the presence of the dipole and quadrupole random errors and magnet alignment errors, the $\beta$ function around the FMI is different from that of an ideal lattice. A typical variation is shown in Figure 5. Figs 6,7 show the distribution of the maximum of horizontal and vertical $\Delta\beta/\beta$ when all the errors are included at 8.9 GeV and 120 GeV. Most of these variations are due to the random errors in the strength of the magnetic elements. The average deviation is about 7%.

*B. Dynamical Aperture*

We have studied the survival of particles launched at different amplitudes in the Main Injector at the injection energy. A single particle in FMI will circulate for a time equivalent to 35000 turns at the injection energy of 8.9 GeV during any operation that involves filling the ring with six bunches coming from the Booster. At 120 GeV where slow extraction of the proton beam is planned the beam will stay in the ring for 1.0 sec at flattop, approximately 100,000 turns. Synchroton oscillation were included in the simulation by launching all particles with an momentum offset of $\delta_{max} = (\Delta p/p)_{max} = 2.0 \times E - 3$ at 8.9 GeV and $0.33 \times E - 3$ at 120 GeV. The maximum beta function of the FMI lattice for a particular seed is less than 65m about 12% larger than the beta function with no errors. We have not found a random number seed which can produce a larger variation in beta function. Particles were launched with a maximum horizontal displacement "A" defined at a location where the horizontal beta function is at its maximum. We have conservatively assumed the maximum beta to be 75 meters. The maximum vertical displacement of the same particle is 0.4A (x/y=2.5), which is the most likely location of the particles. Particles with amplitude varying from 15 mm to 35 mm were considered. Simulations were performed for five different seeds. Figs 8,9 are survival plots displaying how many turns a particle survives in the Main Injector at 8.9 and 120 GeV as a function of initial amplitude. If the dynamical aperture of the machine is defined as the smallest amplitude particle that did not survive the maximum number of turns, then the dynamical aperture for the Main Injector at the injection energy is predicted to be $34.4 \pm 0.8$ mm, corresponding to a normalized emittance of $96.8 \pm 4.5\pi$ mm-mradians.

### *C. Detuning of Particles*

Next we examine the variation of the horizontal and vertical tunes as the amplitude of motion was increased. Figs 10,11 are the tune tune plot at 8.9 and 120 GeV respectively. The numbers on the tune plot corresponds to the initial amplitude "A" of a test particle, in millimeters. Points on the plots lie on a straight line up to an amplitude of 28mm for 8.9 GeV and 31mm for 120 GeV. For 8.9 GeV there is a change in slope for amplitude larger than 28mm. At both of these energies the change in tune is negligible for particles with small amplitude (less than 10mm). It increases but remains uniform for large amplitude particles. This detuning is dominated by a combination of systematic octupole error in the recycled Main Ring quadrupoles, and second order sextupole effects. Half of this detuning is due to the octupole multipole of the quadrupoles.

## III. Correction Schemes

In the FMI lattice there are 54 octupoles and 16 trim quadrupoles placed around the ring for extraction. At present there are 8 additional octupoles correctors in the ring that can be used for a correction scheme. The Main Ring quadrupoles have a positive octupole component which is one of the limiting factor in the dynamical aperture of FMI. The extraction and corrector octupoles will be used to cancel the total effect of this octupole, although in the ring we have now introduced more discrete octupoles. These magnets will have a bipolar power supply. This will enable us to use them as correctors at all the energies except for slow extraction.

In the FMI, the focusing and defocusing quadrupoles are powered by separate power supplies, so the currents of the two circuits can be different. All the recycled Main Ring quadrupoles will be remeasured and reworked before they are placed in the FMI. Knowing the strength of all quadrupoles, will allow us to decide on a scheme of their placement in the ring. The quadrupoles will be divided into two groups. One set will have quadrupoles strength higher than the mean value and the other set lower. This division will reduce the sigma of quadrupole random error by creating two non gaussian distributions. We have used a Monte Carlo simulation to generate a gaussian distribution of quadrupole strength. The sigma of this distribution was chosen to be the sigma derived for best available measurements of the Main Ring quadrupoles. The quadrupoles with strength larger than the mean value were placed on the focusing bus, whereas quadrupoles with

lower strength were placed on the defocussing bus. This reduced the $\Delta\beta/\beta$ of the FMI by a small amount. Further sorting of the quadrupoles by placing pairs of strong or weak quadrupoles exactly one FODO cell apart can reduce this variation in beta function. The variation in $\Delta\beta/\beta$ can be reduced by canceling the natural half-integer stopband of the FMI [4]. This is achieved by using the two family of 16 trim quadrupoles placed in the ring for slow extraction. These trim quadrupoles can be used as correctors at all the energies and as extraction elements for slow extraction. Figure 5 shows the $\Delta\beta/\beta$ of the FMI before any correction is applied. Figure 12 is a similar plot after the quadrupole shuffling to reduce the random error, half-integer stopband and octupole corrections. Figure 13 shows the detuning of the particle at 120 GeV after the quadrupole random error and octupole corrections. Detuning is very small for small amplitude particles. Detuning of large amplitude particle is reduced by about 30%.

Octupole and trim quadrupole correctors are placed in the ring for slow extraction. They will be kept at one current at all energies. For slow extraction these magnets will be ramped through zero to other polarity. This will provide the needed quadrupole and octupole strength for a more stable slow extraction .

The dynamical aperture can be a limiting factor only at the slow extraction, where the horizontal tune of the FMI is changed from 26.425 to 26.485. We have studied the survival of particles for one seed only at the slow extraction tune of $(Q_x, Q_y) = (26.485, 25.425)$ with these corrections. Figure 14 is the survival plot before and after this correction. The dynamical aperture increases by about 7mm. This is mainly due to reduced $\Delta\beta/\beta$ and smaller total octupole in the FMI.

## IV. CONCLUSION

Calculations have shown that the Main Injector design exceeds the design specification of $40\pi$ mm mradians admittance at injection. The larger octupole and the random variation of the quadrupole strengths are the limiting factor for the dynamical aperture at slow extraction. Using a corrector schemes described in this paper it is possible to reduce the effect of the quadrupole random error and octupole multipole. This correction scheme provides us with additional aperture at all energies.

## V. ACKNOWLEDGMENTS

We thank R. Talman for his help with the tracking code TEAPOT. We also thank Steve Holmes, Phil Martin and Steve Peggs for discussions throughout this study.

## V. REFERENCES

[1] L. Schachinger and R. Talman, Particle Accl. 22, 35(1987).

[2] C. S. Mishra, H. D. Glass and F. A. Harfoush, "Effective Length of the Main Injector Dipole and its Effect on Main Injector," Fermilab Main Injector Internal Notes *MI -0072* and H. D. Glass et al, FERMI-TM-1815,1992.

[3] F. A. Harfoush and C. S. Mishra, "Systematic and Random Errors for Main Injector Tracking," Fermilab Main Injector Internal Notes, *MI-0066*, and in the proceedings of PAC93, Washington May 1993 .

[4] J. A. Johnstone, Private Communication.

| Magnet Type | Multipole Order | Normal Errors | | Skew Errors | |
|---|---|---|---|---|---|
| | | $< b_n >$ | $\sigma b_n$ | $< a_n >$ | $\sigma a_n$ |
| Dipole Body | dipole | -4.68 | 10.0 | – | – |
| | quad | -0.13 | 0.45 | – | – |
| | sext | 0.43 | 0.61 | -0.04 | 0.22 |
| | 8 | 0.09 | 0.13 | 0.00 | 0.41 |
| | 10 | 0.18 | 0.32 | 0.03 | 0.15 |
| | 12 | -0.03 | 0.10 | 0.00 | 0.19 |
| | 14 | -0.01 | 0.23 | -0.05 | 0.08 |
| Dipole End | dipole | 2.02 | – | 0.00 | – |
| | quad | 0.03 | – | – | – |
| | sext | 0.256 | – | 0.03 | – |
| | 8 | -0.021 | – | 0.02 | – |
| | 10 | -0.095 | – | 0.00 | – |
| | 12 | 0.009 | – | -0.03 | – |
| | 14 | 0.002 | – | 0.00 | – |
| MR Quads (Recycled) | quad | – | 24.0 | – | – |
| | sext | 0.50 | 2.73 | 0.12 | 1.85 |
| | oct | 5.85 | 1.02 | -1.16 | 2.38 |
| | 10 | -0.10 | 1.12 | 0.42 | 0.47 |
| | 12 | -1.82 | 0.63 | 0.40 | 0.70 |
| | 14 | 0.21 | 0.64 | -0.55 | 0.44 |
| | 16 | 1.41 | 0.64 | – | – |
| | 18 | -0.03 | 0.12 | 0.14 | 0.16 |
| | 20 | -0.80 | 0.06 | 0.02 | 0.07 |
| MI Quads (Newly built) | quad | – | 24.0 | – | – |
| | sext | – | 2.73 | – | – |
| | oct | -0.39 | 1.02 | – | – |
| | 10 | – | 1.12 | – | – |
| | 12 | -1.39 | 0.63 | – | – |
| | 14 | – | 0.64 | – | – |
| | 16 | 1.29 | 0.64 | – | – |
| | 18 | – | 0.12 | – | – |
| | 20 | -0.73 | 0.06 | – | – |

Table 1: Magnetic errors used in the 8.9 GeV simulation (see ref - 3 for details & units)

| Magnet Type | Multipole Order | Normal Errors | | Skew Errors | |
|---|---|---|---|---|---|
| | | $< b_n >$ | $\sigma b_n$ | $< a_n >$ | $\sigma a_n$ |
| Dipole Body | dipole | 0.00 | 10.0 | – | – |
| | quad | -0.30 | 0.21 | – | – |
| | sext | -1.16 | 0.49 | -0.03 | 0.17 |
| | 8 | 0.02 | 0.06 | -0.02 | 0.29 |
| | 10 | -0.09 | 0.25 | -0.04 | 0.07 |
| | 12 | -0.04 | 0.06 | -0.01 | 0.21 |
| | 14 | -0.08 | 0.25 | -0.05 | 0.08 |
| Dipole End | dipole | 0.00 | – | 0.00 | – |
| | quad | 0.08 | – | – | – |
| | sext | -0.52 | – | 0.05 | – |
| | 8 | -0.012 | – | 0.02 | – |
| | 10 | 0.084 | – | 0.05 | – |
| | 12 | 0.008 | – | -0.03 | – |
| | 14 | -0.021 | – | 0.01 | – |
| MR Quads (Recycled) | quad | – | 24.0 | – | – |
| | sext | 1.69 | 2.29 | -0.47 | 3.14 |
| | oct | 5.29 | 1.29 | 0.68 | 0.43 |
| | 10 | -0.72 | 0.90 | 0.41 | 0.34 |
| | 12 | -1.71 | 0.16 | -0.31 | 0.14 |
| | 14 | -0.25 | 0.92 | -0.02 | 1.11 |
| | 16 | 1.37 | 0.92 | – | – |
| | 18 | -0.22 | 0.92 | 0.06 | 0.25 |
| | 20 | -0.82 | 0.33 | -0.05 | 0.08 |
| MI Quads (Newly built) | quad | – | 24.0 | – | – |
| | sext | – | 2.29 | – | – |
| | oct | -0.10 | 1.29 | – | – |
| | 10 | – | 0.90 | – | – |
| | 12 | -1.41 | 0.16 | – | – |
| | 14 | – | 0.92 | – | – |
| | 16 | 1.32 | 0.92 | – | – |
| | 18 | – | 0.92 | – | – |
| | 20 | -0.74 | 0.33 | – | – |

Table 2: Magnetic errors used in the 120 GeV simulation (see ref-3 for details & units)

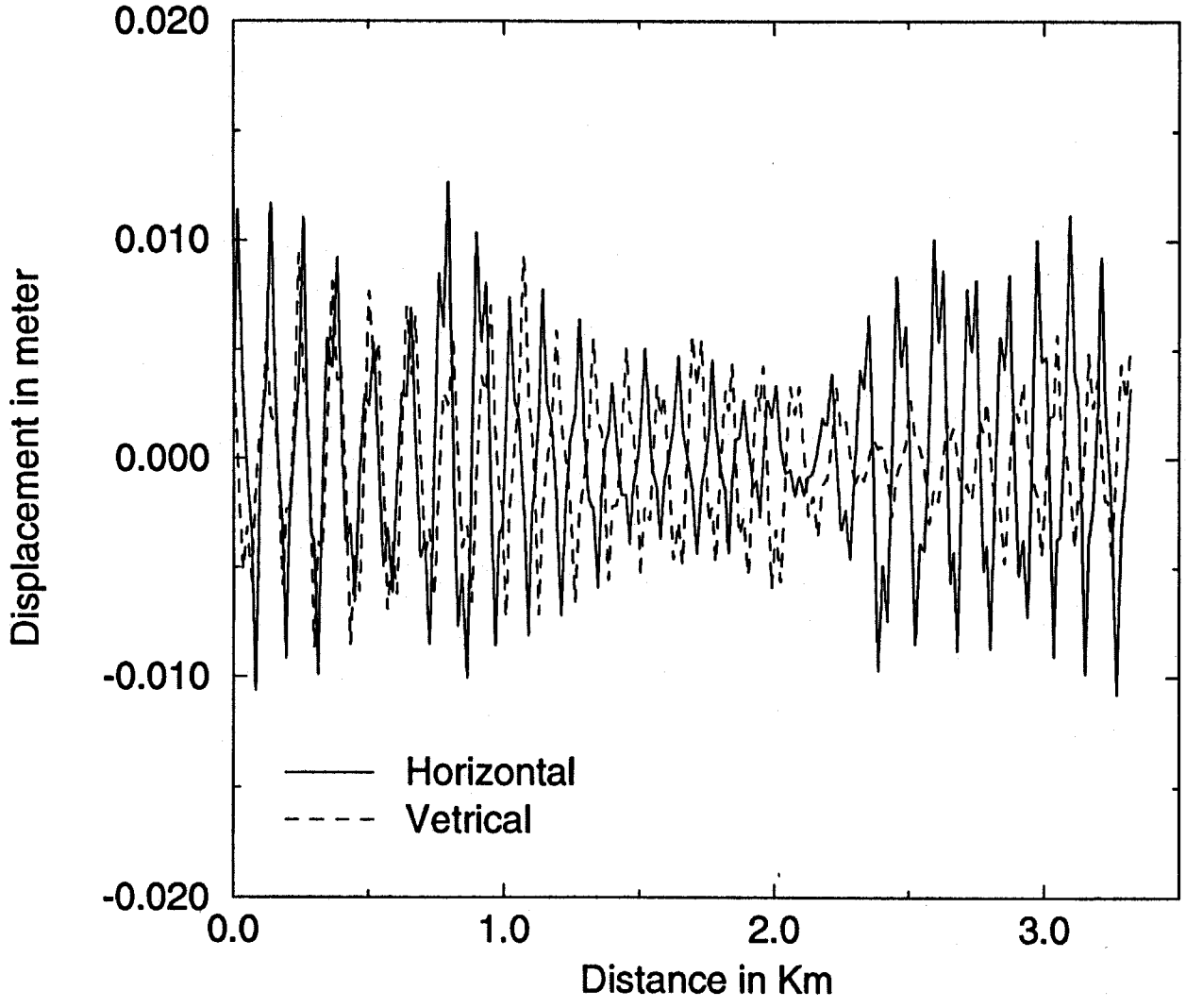


Figure 1: Typical orbit in both planes before correction

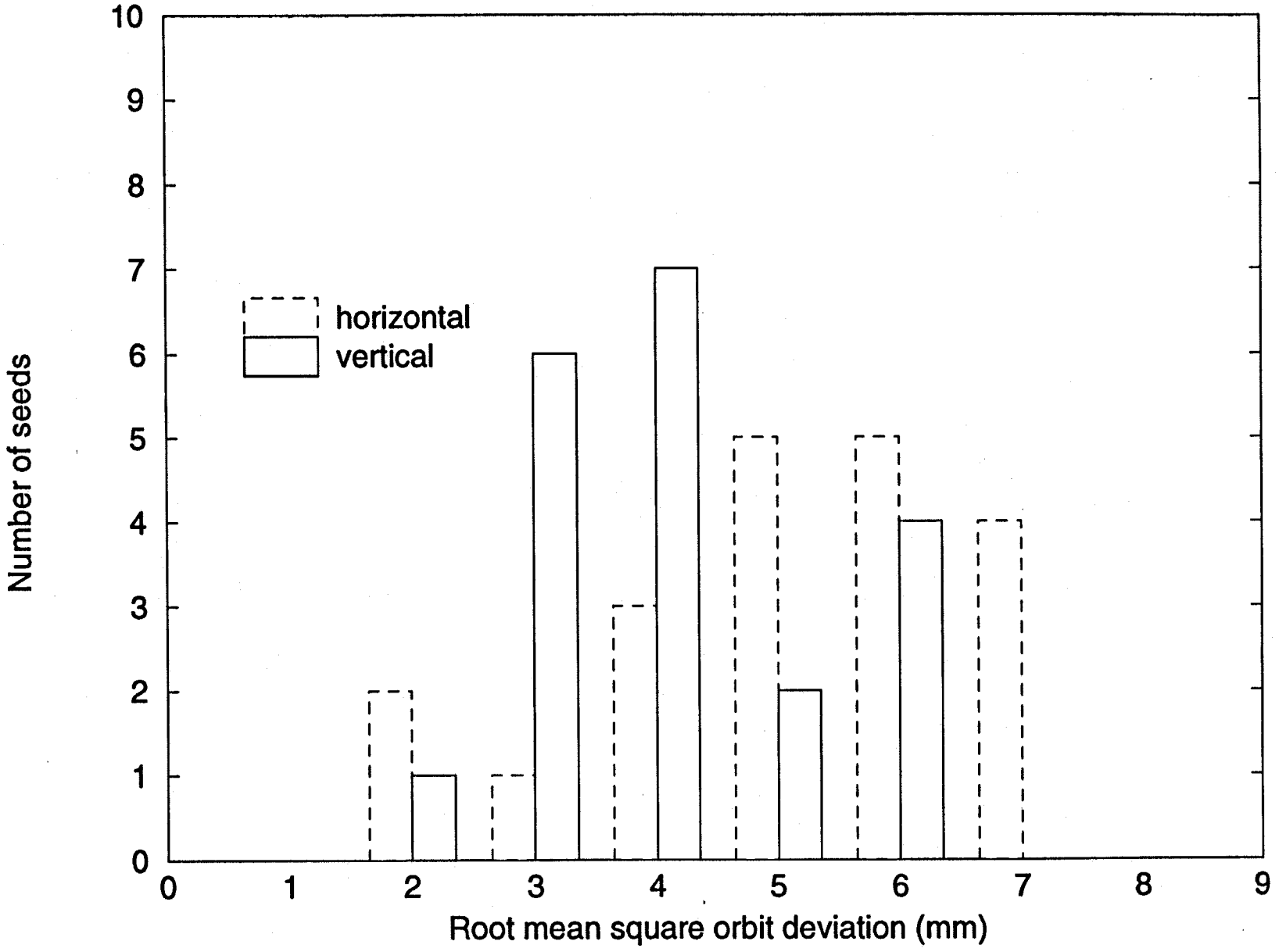


Figure 2: Histogram of closed orbit errors before correction at 8.9 GeV

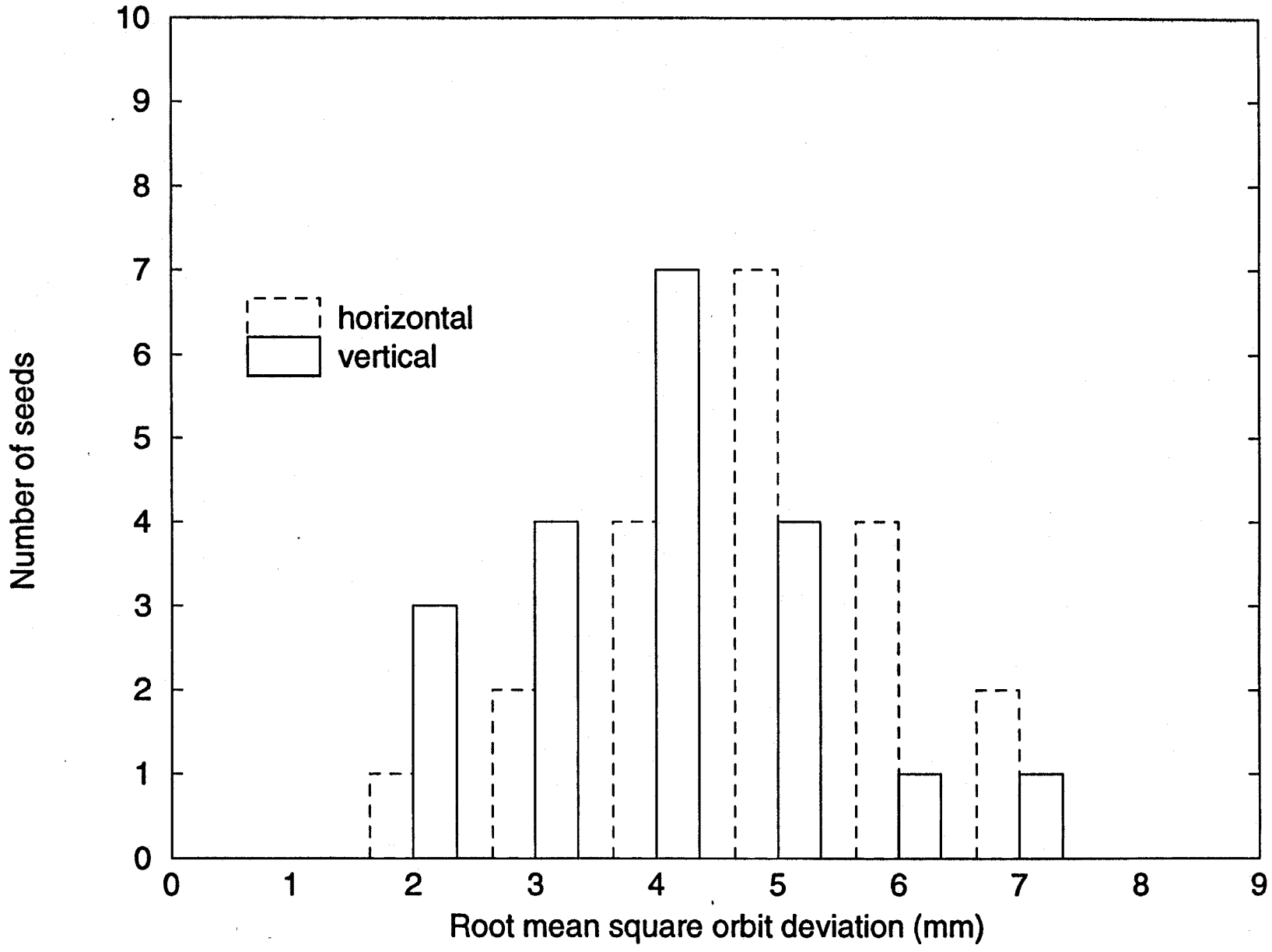


Figure 3: Histogram of closed orbit errors before correction at 120 GeV

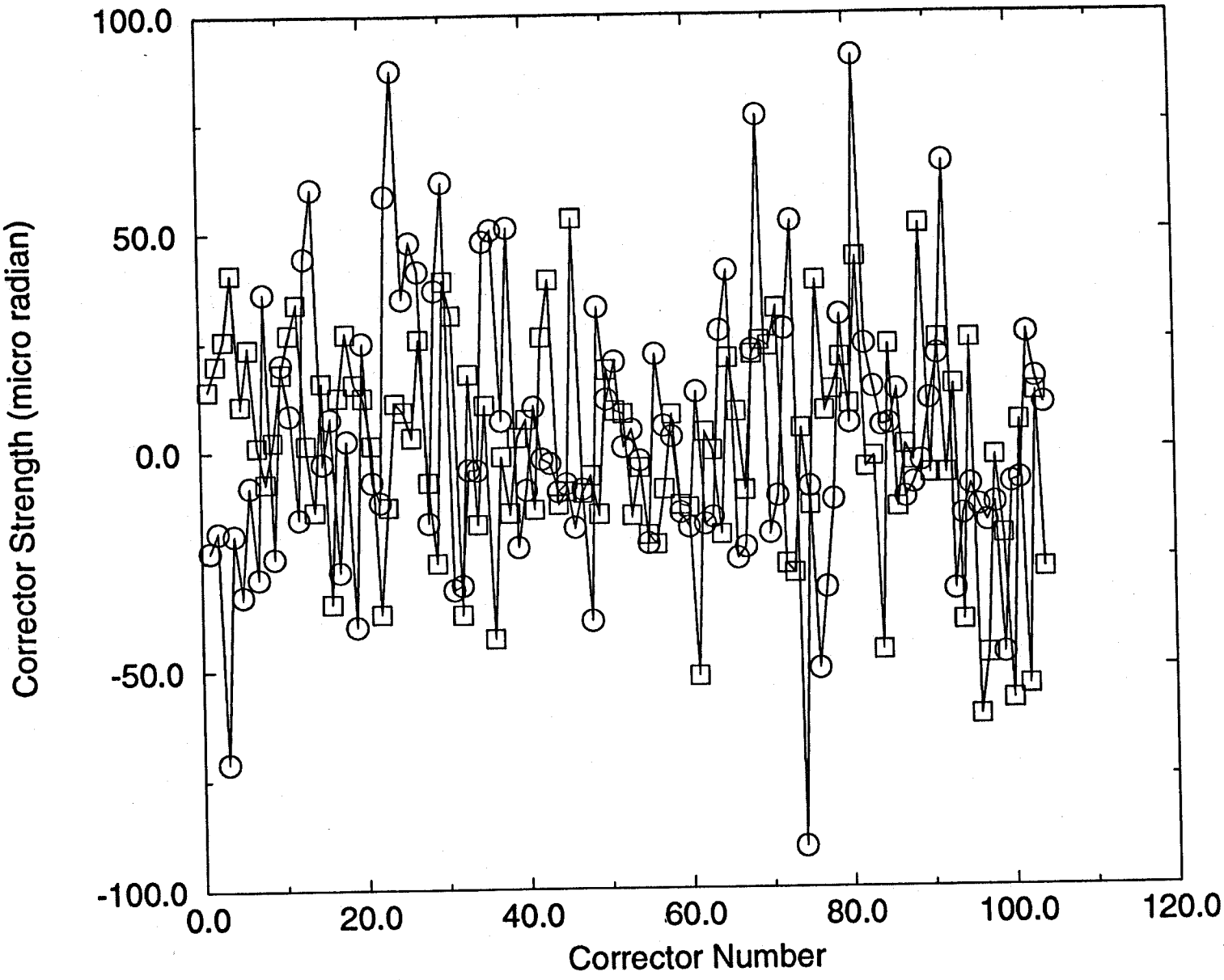


Figure 4: Correctors strength at 8.9 GeV

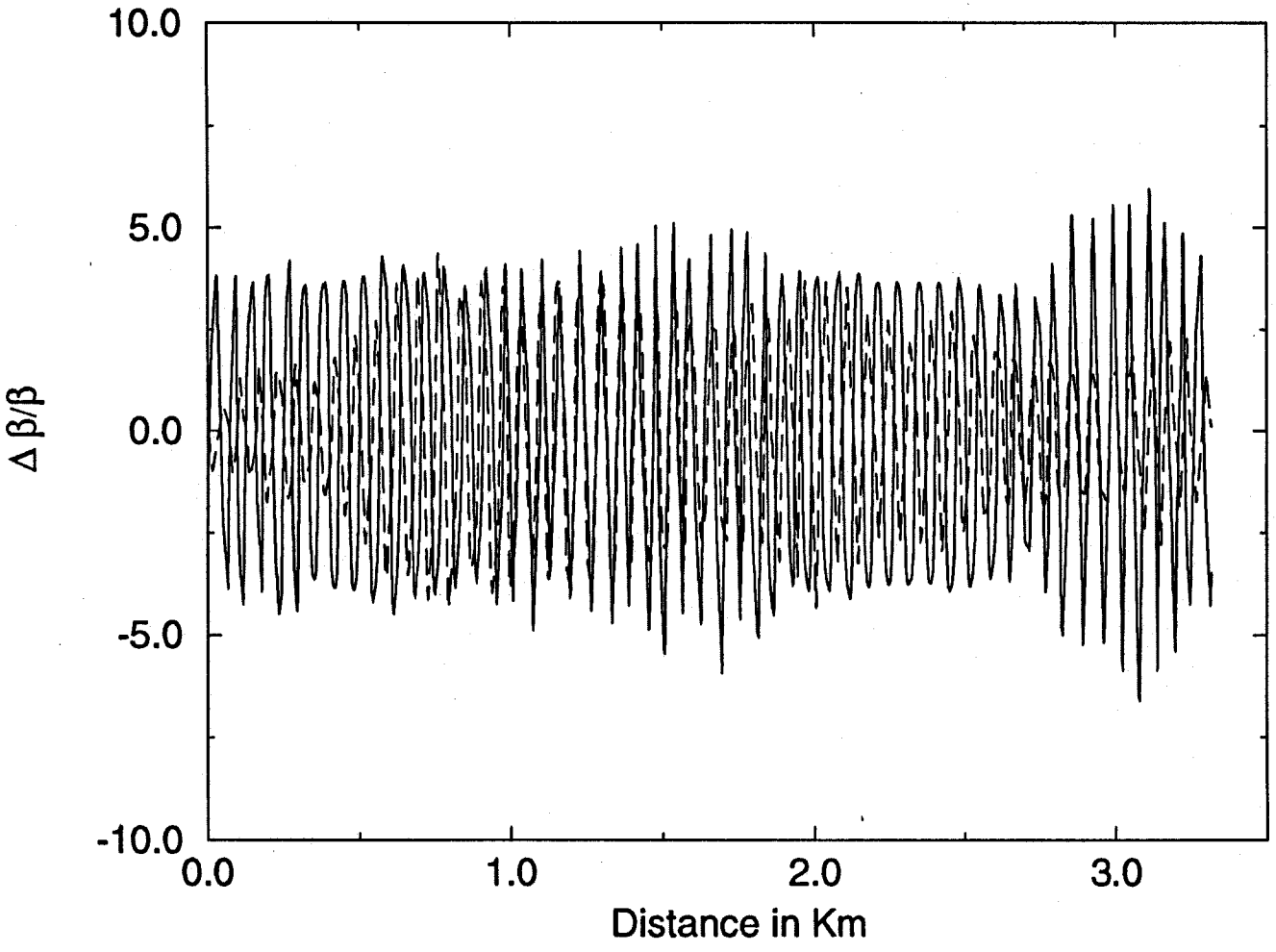


Figure 5: Typical beta function variation before any correction scheme

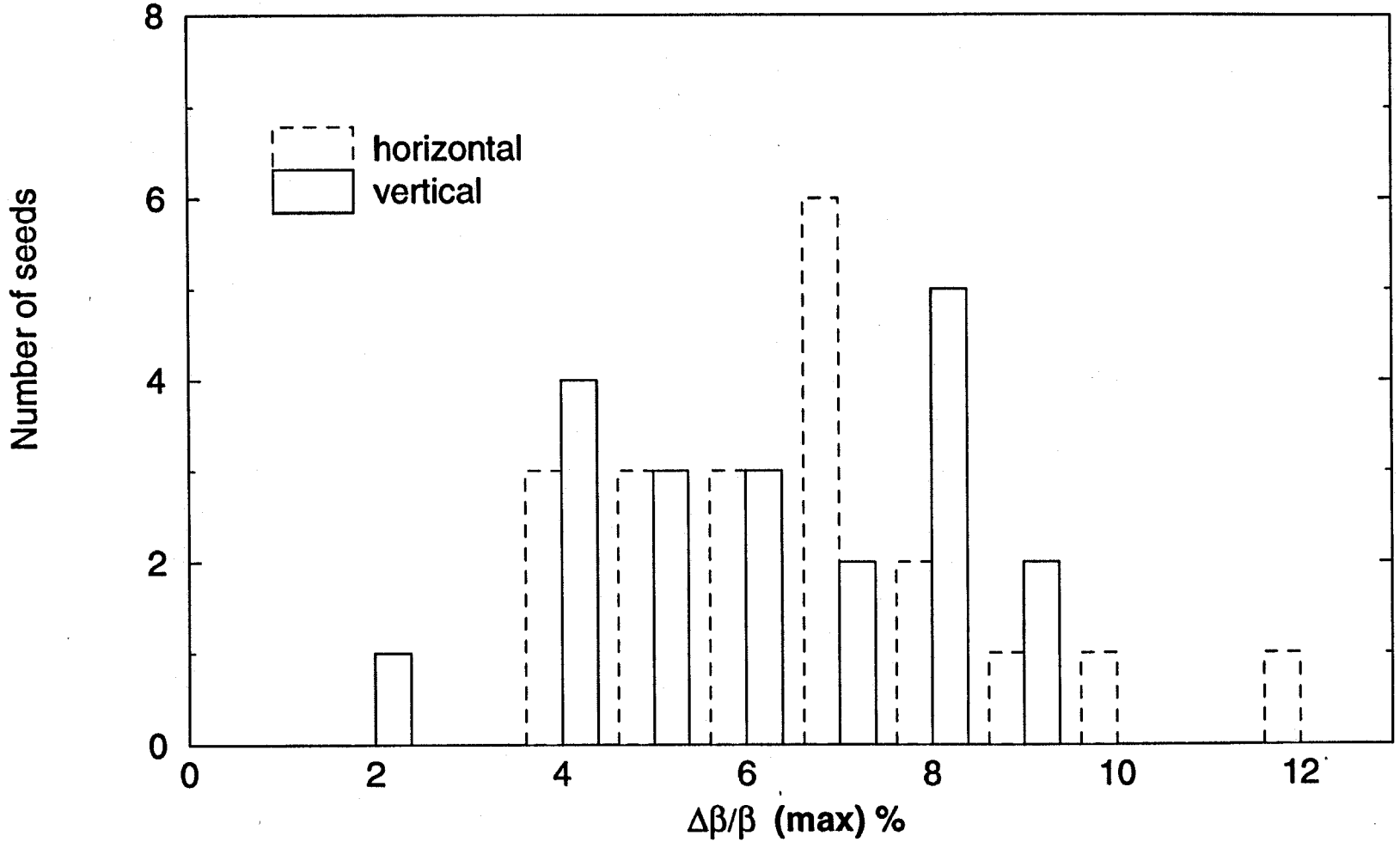


Figure 6: Histogram of beta maximum variations at 8.9 GeV

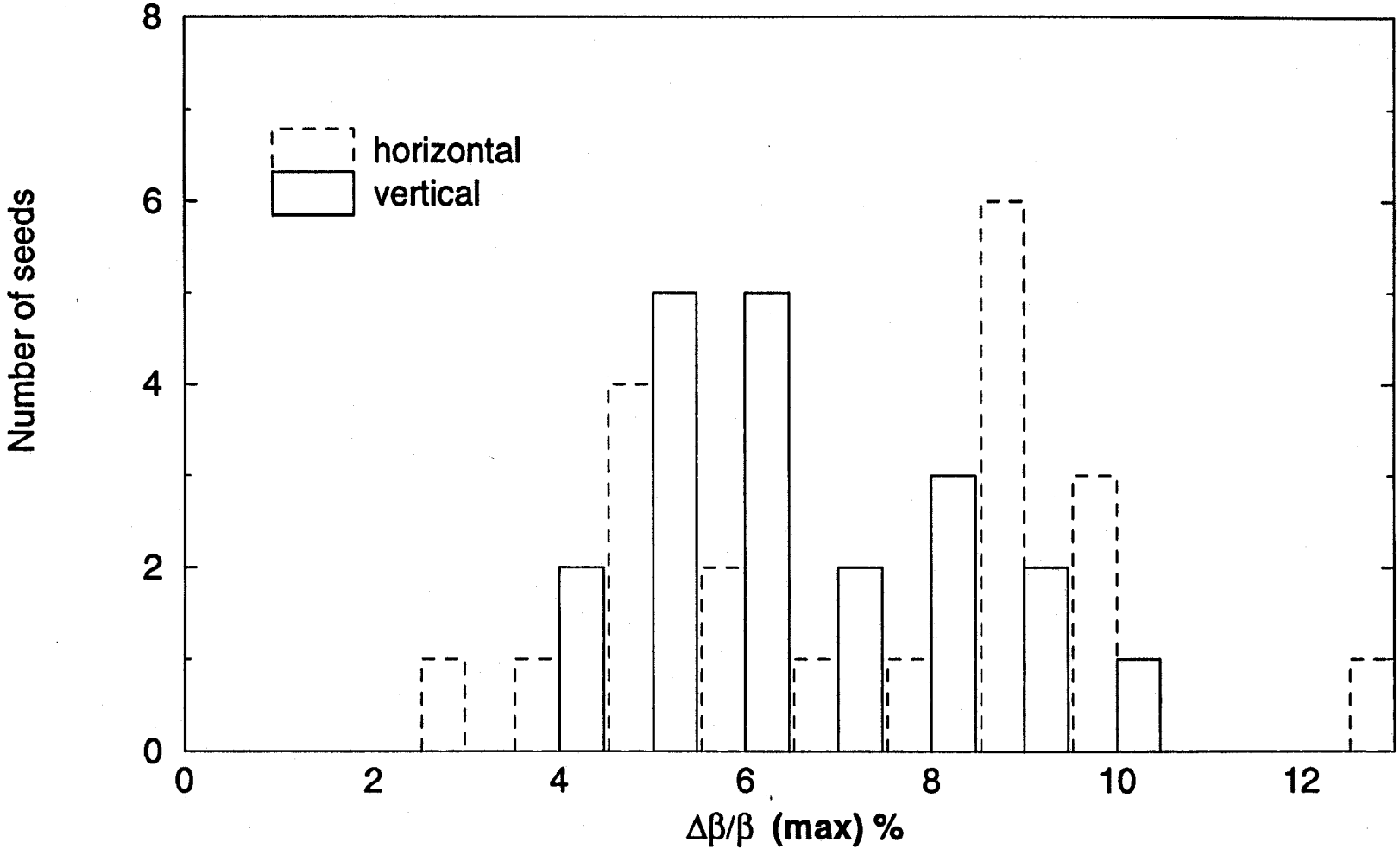


Figure 7: Histogram of beta maximum variations at 120 GeV

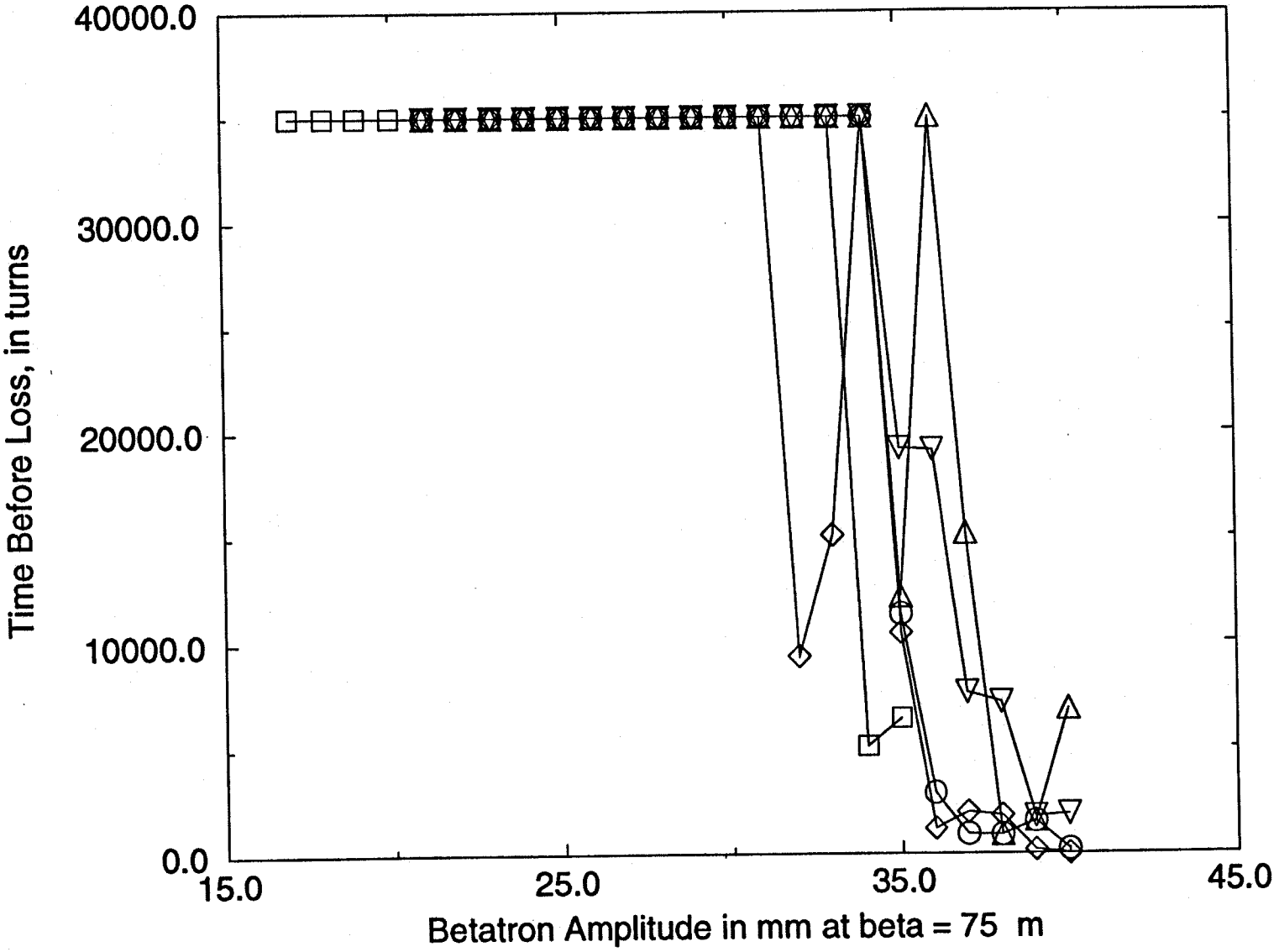


Figure 8: Survival plot at 8.9 GeV

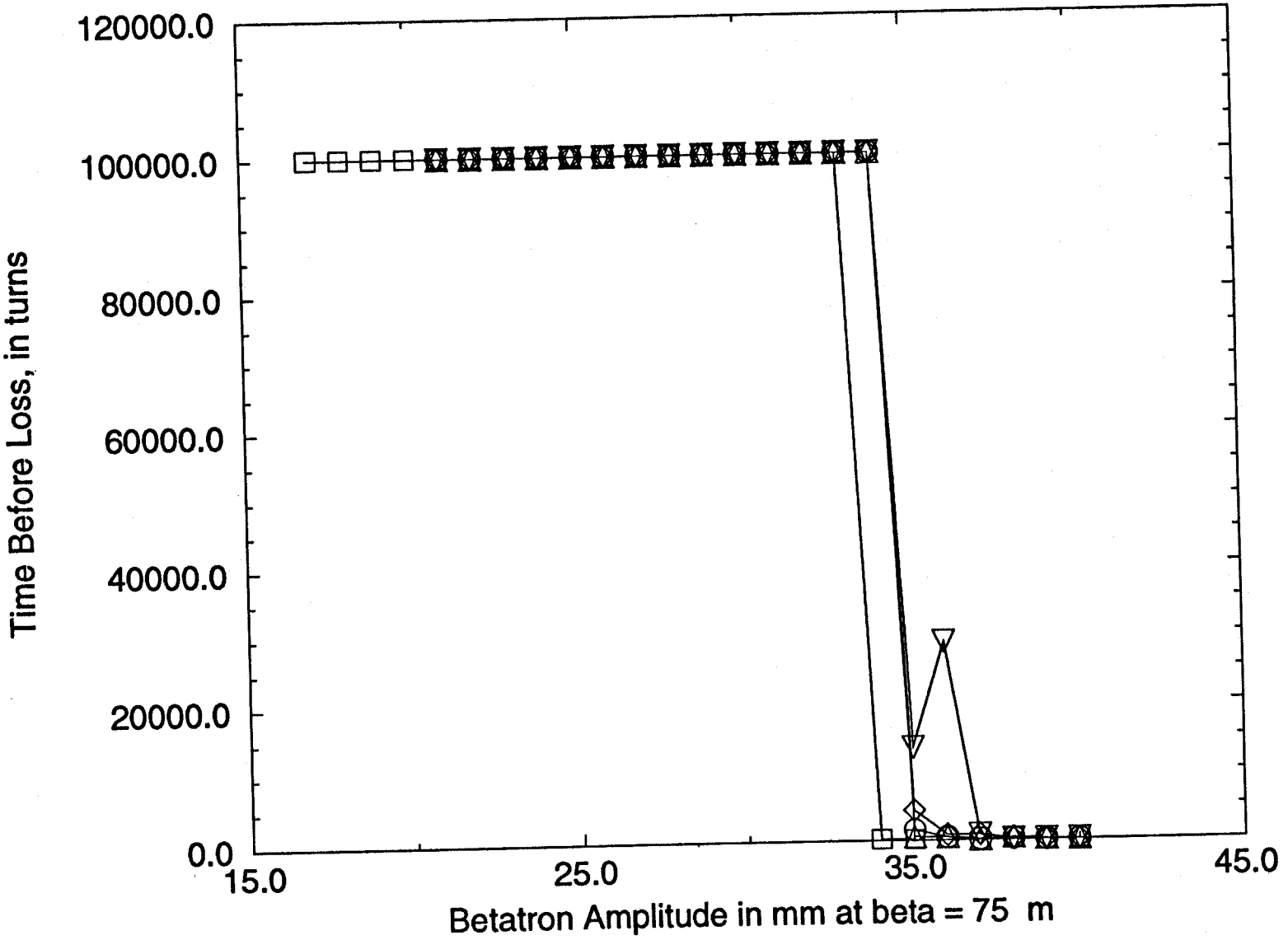


Figure 9: Survival plot at 120 GeV

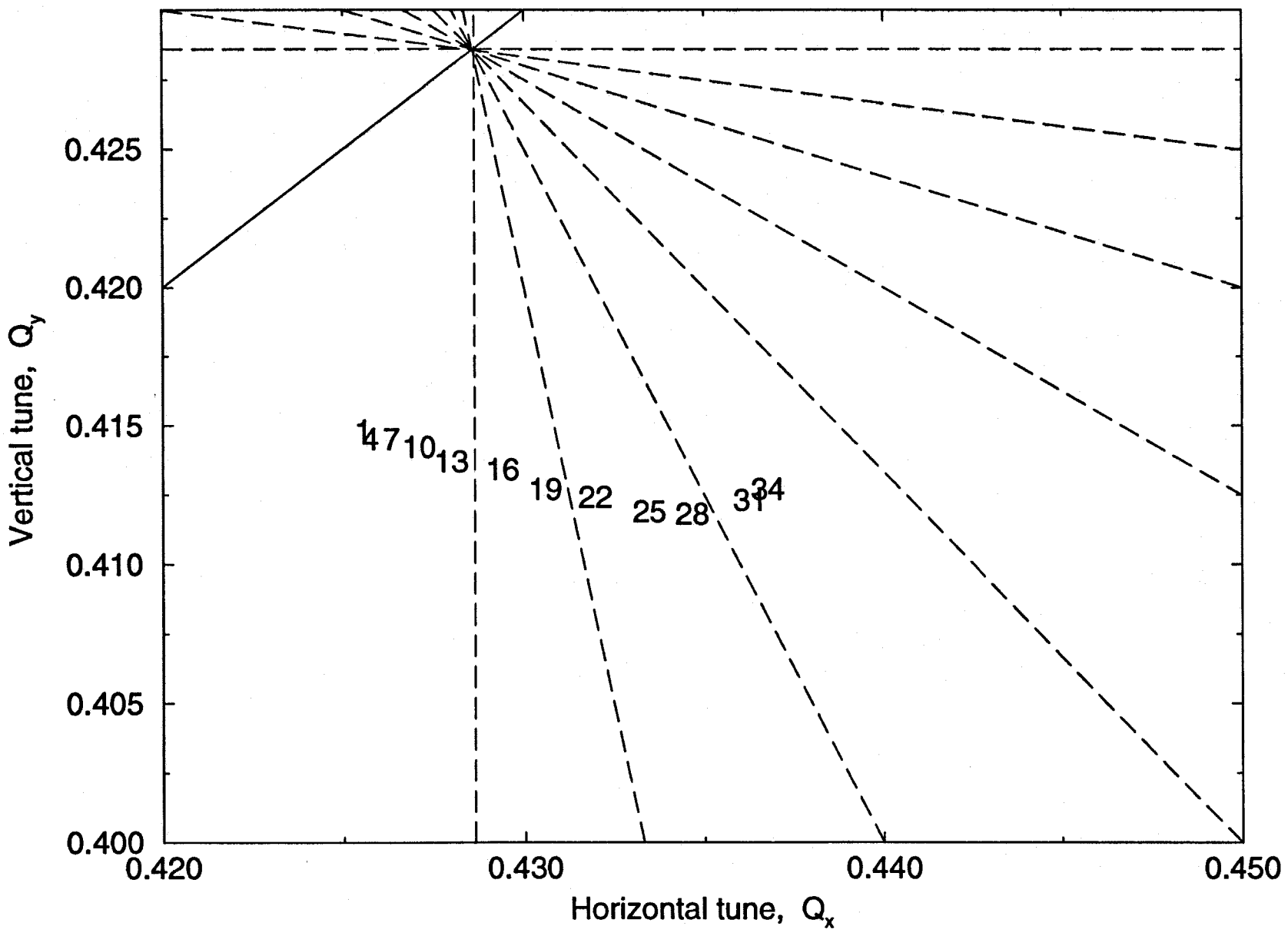


Figure 10: Tune-tune plot at 8.9 GeV

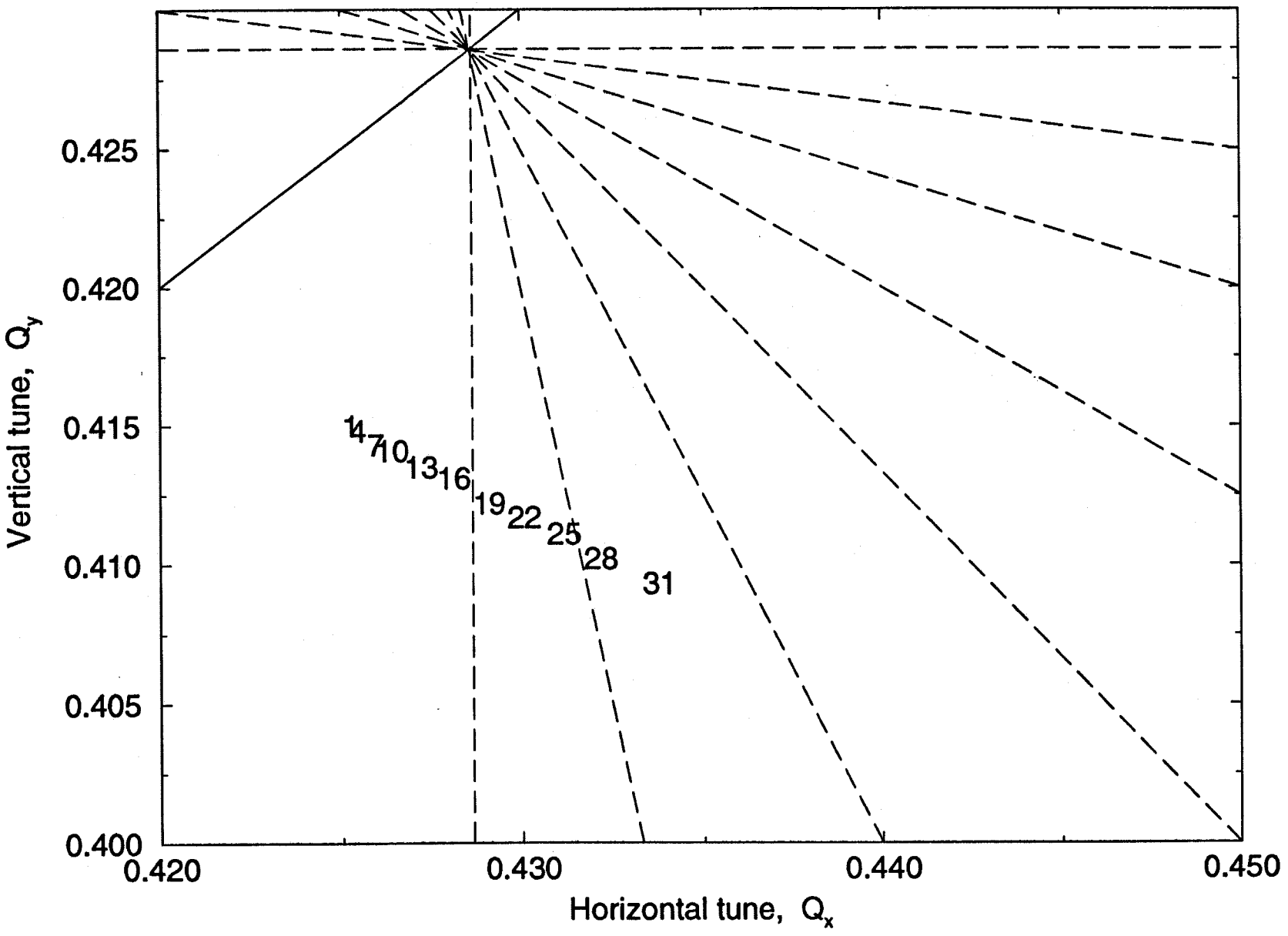


Figure 11: Tune-tune plot at 120 GeV

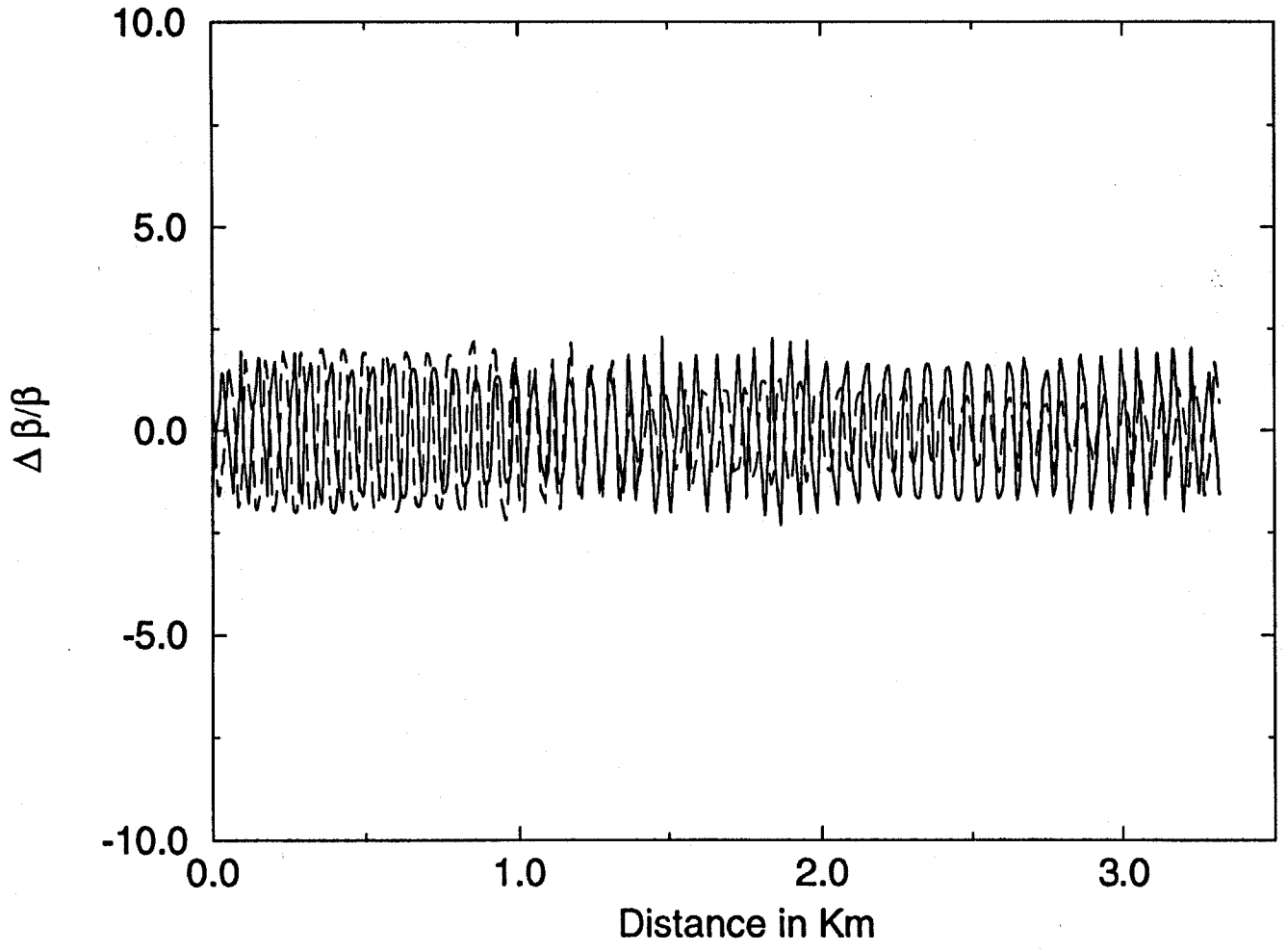


Figure 12: Beta function variations after corrections at 120 GeV

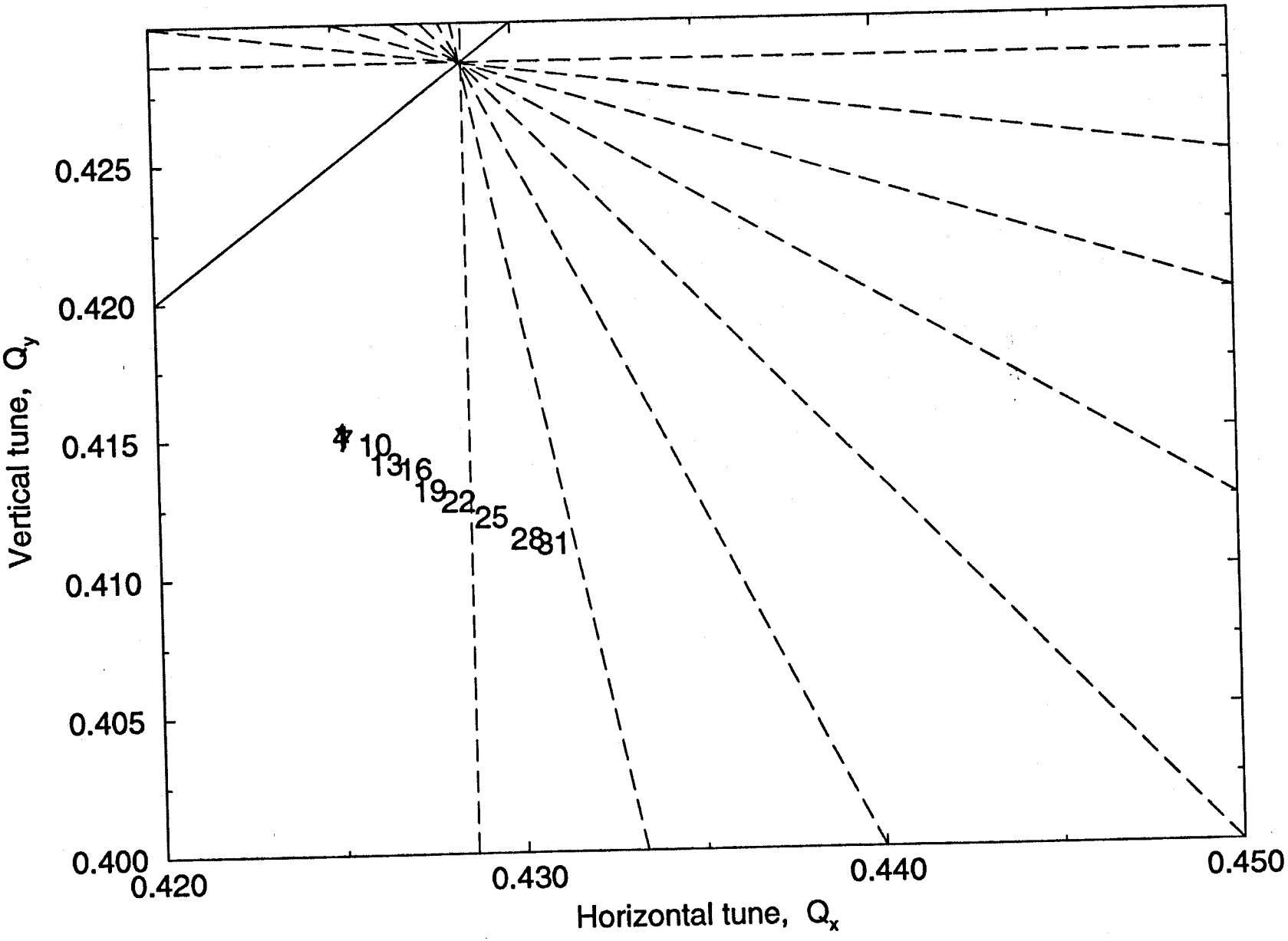


Figure 13: Tune-tune plot at 120 GeV after corrections

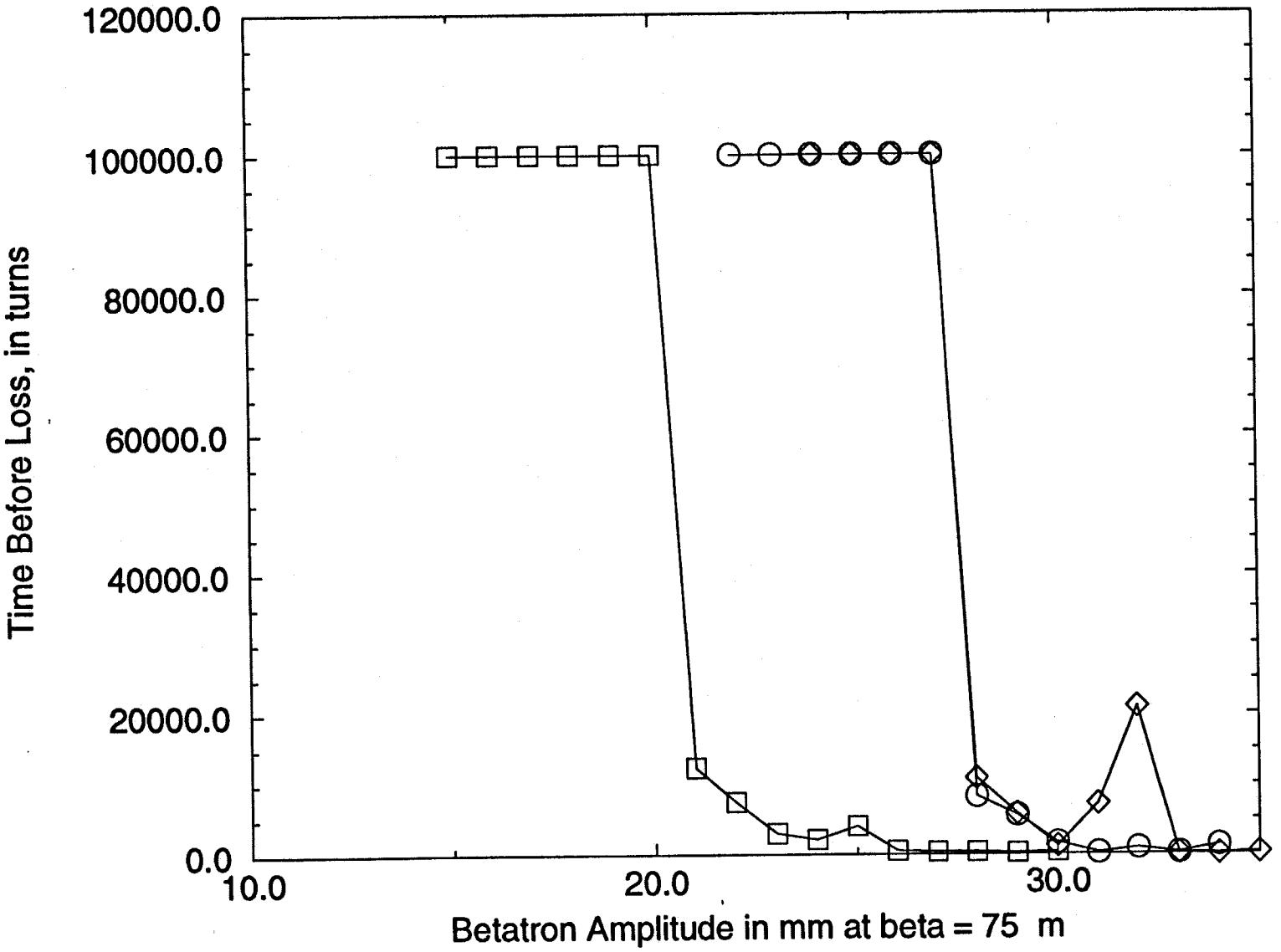


Figure 14: Survival plot after corrections at 120 GeV